Inorganic Chemistry

pubs.acs.org/IC

Article

Stable Cd Metal–Organic Framework as a Multiresponsive Luminescent Biosensor for Rapid, Accurate, and Recyclable Detection of Hippuric Acid, Nucleoside Phosphates, and Fe^{3+} in Urine and Serum

Mingyuan Lei, Fayuan Ge, and Hegen Zheng*

Cite This: *Inorg. Chem.* 2022, 61, 11243–11251

Read Online

ACCESS | Metrics & More | Article Recommendations | Supporting Information

ABSTRACT: Detecting biomarkers associated with diseases has significant meaning for early prevention, diagnosis, and treatment of diseases. The development of luminescent biosensors for rapid and accurate detection in real urine and serum is urgently desired for human health monitoring. Herein, a luminescent cadmium metal–organic framework, $\{[Cd(L)(bpbix)]\cdot x(solv)\}_n$ (**1**), was successfully prepared by using a urea-functionalized dicarboxylate ligand, 5-(3-(pyridin-4-yl)ureido)isophthalic acid (H_2L), 4,4′-bis((1*H*-imidazol-1-yl)methyl)biphenyl (bpbix), and the Cd^{2+} ion. The structure of **1** presents a 2-fold interpenetrating three-dimensional pillared-layer framework. The complex **1** exhibits good stability in different-pH aqueous solutions and physiological fluids. Strikingly, the complex **1** shows quick response, high sensitivity, good anti-interference performance, and a recyclable ability for simultaneous sensing of hippuric acid (HA), nucleoside phosphates, and Fe^{3+} in water. More significantly, this sensor can realize the sensitive and accurate detection of HA, nucleoside phosphates, and Fe^{3+} in real urine and serum and meet the practical detection needs in clinical diagnosis. These results indicate that the complex **1** as a multiresponsive luminescent biosensor possesses great potential for practical detection of HA, nucleoside phosphates, and Fe^{3+} in biological samples.

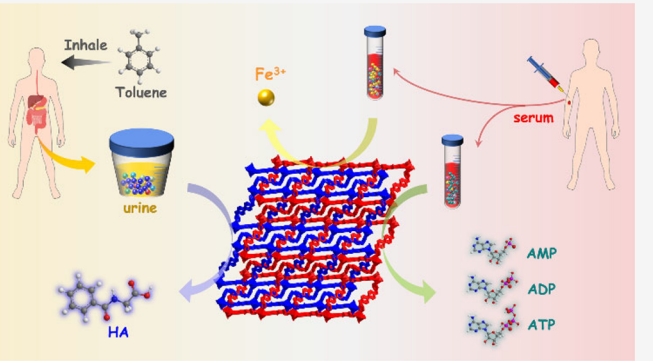

1. INTRODUCTION

Biomarkers are crucial indicators that can determine the occurrence and stage of diseases, which also play a key role in disease prevention, early diagnosis, and treatment. For example, toluene is a common organic solvent and widely used in printing, painting, automotive, pharmaceutical, and petroleum industries in many countries.[1,2] However, long-term exposure to toluene does harm to the human brain and the central nervous system.[2] Therefore, monitoring of the toluene level in a working environment is of great significance for the health of workers. However, due to individual differences, the content of toluene in the environment cannot precisely and truly reflect its real level in the human body.[3] According to a study, more than 80% of toluene inhaled by humans is metabolized to hippuric acid (HA) followed by excretion in urine, and the urinary concentration of HA is proportional to the exposure level of toluene.[4] So, the urinary HA is considered to be an important biomarker in the monitoring of the level of toluene exposure in the human body. In addition, nucleoside phosphates including adenosine monophosphate (AMP), adenosine diphosphate (ADP), and adenosine triphosphate (ATP) play a vital role in numerous biological processes including metabolism, energy storage and transduction, genetic information transmission, and protein biosynthesis.[5,6] Imbalance in the concentration of nucleoside phosphates causes many diseases such as malignant tumors, Parkinson's disease, malnutrition, and heart attacks.[7−10] Thus, the nucleoside phosphates can be used as biological indicators for health diagnosis. Equally importantly, the Fe^{3+} ion, as a common metal ion in living organisms, plays a critical role in many physiological processes including oxygen metabolism, electron transfer, and hemoglobin synthesis.[11,12] The deficient or excessive level of Fe^{3+} ion in the human serum can lead to iron deficiency anemia, cancer, and cardiovascular and Alzheimer's diseases.[13,14] Thus, it is imperative to find a new way to accurately monitor the level of various biologically

Received: April 18, 2022
Published: July 14, 2022

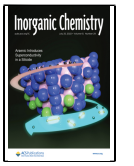

https://doi.org/10.1021/acs.inorgchem.2c01313
Inorg. Chem. 2022, 61, 11243−11251

relevant substances for the prevention of diseases and early diagnosis.

Recently, extensive efforts were devoted to study many methods for detection of HA, nucleoside phosphates, and the Fe^{3+} ion, such as liquid chromatography−tandem mass spectrometry (LC−MS/MS), gas chromatography (GC), capillary electrophoresis (CE), coupled enzyme assays, electrochemical assay, surface-enhanced Raman scattering (SERS), atomic absorption spectrometry, and inductively coupled plasma-mass spectrometry (ICP-MS).[15−22] However, they require time-consuming, complex technologies and large and expensive equipment and exhibit rather poor repeatability. Therefore, it is an important but challenging task to seek a rapid, simple, low-cost, and recyclable way for detection of HA, nucleoside phosphates, and the Fe^{3+} ion in biological media. Compared with the abovementioned techniques, the optical sensing method based on the change in the luminescent intensity caused by host−guest interactions has drawn increasing attention because of its fast response time, easy operation, good sensitivity, and recyclability.[23] Luminescent metal−organic frameworks (MOFs) have found wide promising applications in the field of sensing due to their excellent photoluminescent properties, high surface area, structural tunability, and functionalization.[24] Up to now, an increasing number of luminescent MOF-based sensors have been applied for biosensing.[25,26] However, the reported luminescent MOF-based biosensors only display monoresponsive detection or dual-responsive detection.[3,4,8,10,12−14,27−31] To our knowledge, multiresponsive luminescent MOF-based biosensors for detection of HA, nucleoside phosphates, and the Fe^{3+} ion have been not reported so far. On the other hand, biosensing experiments were rarely performed in human fluids due to the complexity of bodily fluids.[3,10,32−35] This affects the accuracy of detection and hinders the practical application of MOF-based biosensors in disease screening and diagnosis. Thus, it is an urgent need to develop stable multiresponsive luminescent MOF-based biosensors for accurate detection in urine and serum.

It is well-known that the urea group can provide two amide N−H fragments to two oxygen atoms of carboxylic or phosphate groups, forming two strong hydrogen bonds,[36] and N-donor and O-donor atoms of the urea group act as good binding sites for the Fe^{3+} ion.[37] Thus, the urea group offers guest-interaction functional sites for the effective detection of HA, nucleoside phosphates, and the Fe^{3+} ion. Herein, a new urea-functionalized ligand, 5-(3-(pyridin-4-yl)ureido)-isophthalic acid (H_2L), was designed and successfully synthesized. The H_2L was used to react with 4,4′-bis((1*H*-imidazol-1-yl)methyl)biphenyl (bpbix) and the Cd^{2+} ion *via* solvothermal conditions to successfully construct a 2-fold interpenetrating 3D pillared-layer Cd-MOF, $\{[Cd(L)(bpbix)]\cdot x(solv)\}_n$ (**1**) (Scheme 1). This MOF simultaneously exhibited good anti-interference performance and rapid, sensitive, and recyclable detection of HA, nucleoside phosphates, and Fe^{3+} in water. Most notably, the complex **1** was able to detect HA, nucleoside phosphates, and Fe^{3+} in real urine and serum with high sensitivity, accuracy, and reliability. Therefore, the complex **1** can be used as a highly promising multiresponsive luminescent biosensor for the simultaneous determination of HA, nucleoside phosphates, and Fe^{3+} in real biological environments.

Scheme 1. Synthesis of the Cd-MOF as a Multiresponsive Luminescent Biosensor for the Simultaneous Sensing of HA, Nucleoside Phosphates, and the Fe^{3+} Ion in Real Urine and Serum

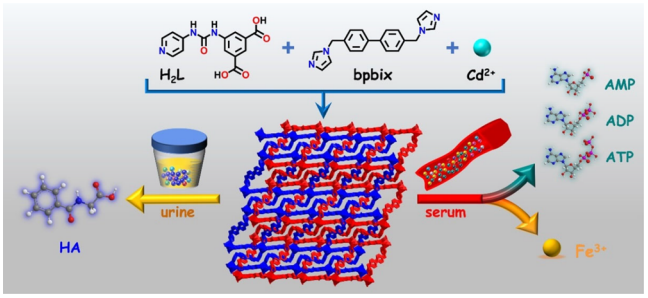

2. EXPERIMENTAL SECTION

2.1. Synthesis of H_2L. A mixture of isonicotinic acid (3 g, 24.37 mmol), triethylamine (3.6 mL, 25.59 mmol), and diphenylphosphoryl azide (5.43 mL, 25.59 mmol) in dry acetonitrile (20 mL) was stirred under a N_2 atmosphere at 0 °C for 30 min and then heated at 75 °C for 2 h. The reaction was cooled down to room temperature, and the solvent was removed. Then, 4-aminobenzoic acid (4.64 g, 25.59 mmol) and *N*,*N*′-dimethylformamide (DMF, 50 mL) were added. The mixture was stirred for 24 h at room temperature, and 300 mL of water was added; finally, 5% HCl was added until the solution was at pH = 1. The faint yellow solid was collected by filtration, washed with water, and dried in air (3.6 g, 49% yield). ^{1}H NMR (500 MHz, DMSO-d_6): δ = 13.27 (s, 2H), 9.43 (s, 1H), 9.33 (s, 1H), 8.39 (d, J = 5 Hz, 2H), 8.28 (s, 2H), 8.13 (s, 1H), 7.47 (d, J = 5 Hz, 2H). IR spectrum (KBr, cm^{-1}): 3035, 2808, 1727, 1689, 1657, 1637, 1586, 1558, 1510, 1434, 1385, 1352, 1320, 1278, 1250, 1212, 1194, 1105, 1046, 969, 899, 824, 789, 761, 742, 708, 654, 604, 562, 518, 451.

2.2. Synthesis of Complex 1. $Cd(NO_3)_2\cdot 4H_2O$ (30.8 mg, 0.1 mmol), H_2L (9.0 mg, 0.03 mmol), and bpbix (9.4 mg, 0.03 mmol) were dissolved in the mixture of 0.5 mL of DMF and 2.5 mL of deionized water by ultrasound. The suspension was sealed and heated at 120 °C for 72 h and then cooled to room temperature. The colorless block-shaped crystals were collected (yield of 68.2% based on H_2L). Elemental analysis for evacuated samples of complex **1** ($C_{34}H_{27}N_7O_5Cd$): C, 56.25; H, 3.75; N, 13.50%. Found: C, 56.52; H, 3.76; N, 13.22%. IR spectrum (KBr, cm^{-1}): 3314, 1645, 1617, 1556, 1521, 1429, 1351, 1315, 1269, 1232, 1198, 1108, 1082, 1007, 933, 899, 797, 778, 739, 654, 530, 484, 446.

2.3. Pretreatments of Urine and Serum Samples. Urine was collected from a healthy member of the research group. A fresh calf serum sample was purchased from Sigma-Aldrich Company. In detail, the urine and serum samples were centrifuged (10,000 rpm/min) for 10 min, and the supernatants of urine and serum were diluted with 100-fold deionized water to eliminate the matrix effect of urine and serum.

2.4. Luminescence Experiments. A 3.0 mg complex **1** sample was dispersed in 10 mL of deionized water and ultrasonicated for 30 min, and then, the obtained suspension was placed in a quartz cuvette. Subsequently, the luminescence detection experiments were performed by gradually adding analyte solutions. The steps of luminescence titration experiments in urine and serum were consistent with those in water.

2.5. Recyclable Luminescence Experiments. The recyclability of **1** for sensing of HA, AMP, ADP, ATP, and Fe^{3+} was studied. After the luminescence experiments, **1** was recovered by centrifugation of the suspension and washing with water several times. The recycled samples were collected and subjected to the next sensing cycle.

3. RESULTS AND DISCUSSION

3.1. Crystal Structure. Single-crystal X-ray diffraction analysis shows that the complex **1** crystallizes in the monoclinic

https://doi.org/10.1021/acs.inorgchem.2c01313
Inorg. Chem. 2022, 61, 11243−11251

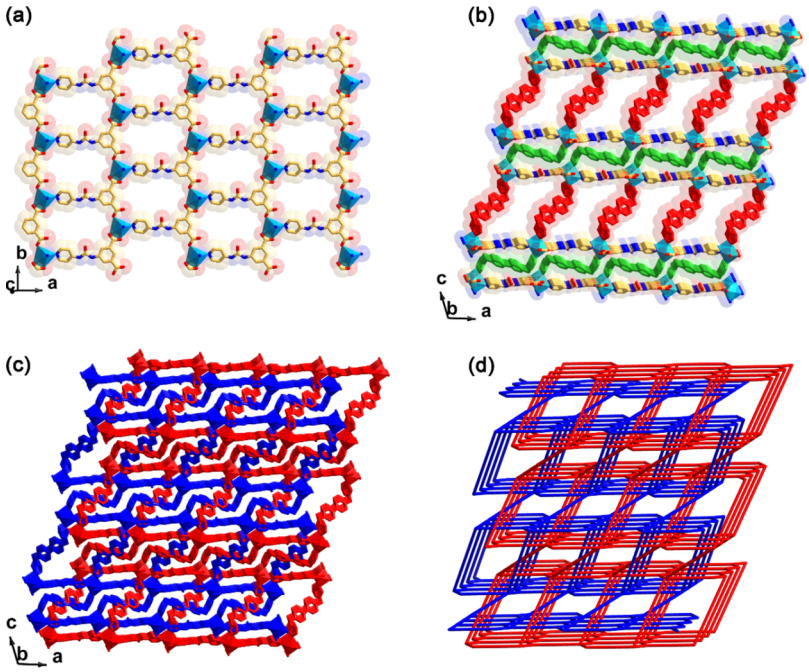

Figure 1. (a) 2D honeycomb layer. (b) Single net of the 3D framework. (c) Twofold interpenetrating 3D structure along the *b* axis. (d) Topological representation of the 2-fold interpenetrating (3,5)-connected **gra** network.

space group $C2/c$ and consists of one Cd^{2+} ion, one L^{2-} ligand, and two half bpbix ligands in the asymmetric unit (Figure S1). Each Cd^{2+} ion is hexa-coordinated by three carboxylate O atoms (O1, O3A, and O4A) from two different L^{2-} ligands, one pyridyl N atom (N1B) from the other L^{2-} ligand, and two apical imidazolyl N atoms (N4 and N6) from two different pillaring bpbix ligands, displaying a distorted $[CdO_3N_3]$ octahedral geometry (Figure S2). The Cd−O/N bond lengths [2.206(3)−2.481(3) Å] fall into the normal range.[38,39]

As shown in Figure 1a, each L^{2-} ligand connects three Cd^{2+} ions, and each Cd^{2+} ion in turn is linked by three L^{2-} ligands, forming a 2D honeycomb layer with hexagonal windows. The adjacent layers are alternately linked by pillared bpbix ligands with two different conformations to afford a pillared-layer 3D framework structure with 1D parallelogram channels (13.6 × 7.7 $Å^2$) along the *b* axis (Figure 1b). Because of the large pores of the single net, structural interpenetration may occur, which significantly enhances the stability of frameworks. As expected, two independent single nets are interpenetrated with one another to give a 2-fold interpenetrating 3D structure (Figure 1c). Topologically, the Cd^{2+} ion, L^{2-}, and bpbix ligands act as 5-, 3-, and 2-connected nodes. So, overall, the 3D framework can be considered as a 2-nodal (3,5)-connected **gra** network with a Schläfli symbol of $(6^3)(6^9{\cdot}8)$ (Figure 1d). After the interpenetration, the total solvent-accessible volume of complex **1** is about 821.7 $Å^3$, which still represents 12.2% of the per unit-cell volume (6708.6 $Å^3$) calculated with PLATON.[40]

3.2. Stability Test. Water is a crucial and essential component of the human body and also exists in the whole biological processes of a human being. Therefore, it is highly necessary to examine the water stability of **1**. The as-synthesized sample was immersed in water at room temperature for 3 days. The PXRD pattern of the water-treated sample of **1** has no obvious changes as compared with that of the pristine sample (Figure 2), indicating the good water

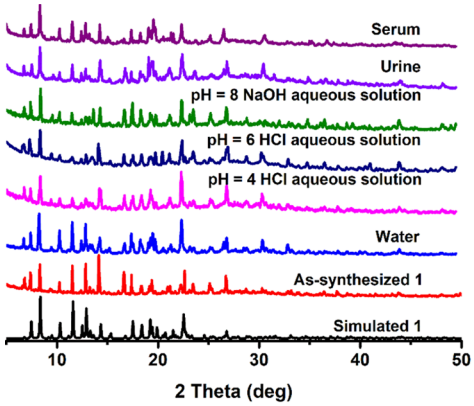

Figure 2. PXRD patterns of **1** after immersion in water, pH = 4−8 aqueous solutions, urine, and serum.

stability of **1**. Because the pH values of the urine and serum are within the normal physiological range (4.6−8),[3,41] the acidic and alkaline stability of **1** is also explored by immersion in pH = 4−8 aqueous solutions for 3 days. The measured PXRD patterns are in agreement with that of the pristine sample (Figure 2), indicating that the complex **1** remains stable after treatments. Moreover, **1** can retain its good crystallinity after immersion in urine and serum (Figure 2). The good stability of **1** makes it competent for practical sensing application in real biological samples. Furthermore, inductively coupled plasma-optical emission spectrometry (ICP-OES) of the supernatants after the above treatment was also checked, and no obvious Cd^{2+} leaching from the Cd-MOF into solution was observed (Table S3), which further confirms the good structural stability. In addition, the thermal stability of **1** was analyzed by thermogravimetric analysis (TGA). The result indicates that the decomposition temperature is up to *ca.* 295 °C (Figure S6), indicating the good thermal stability of **1**. The good

https://doi.org/10.1021/acs.inorgchem.2c01313
Inorg. Chem. 2022, 61, 11243−11251

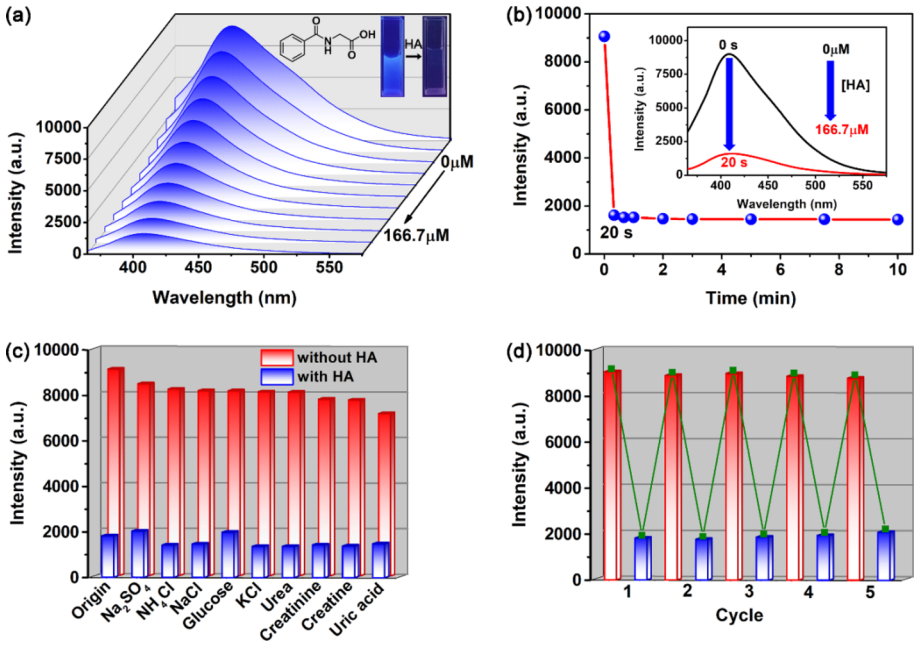

Figure 3. (a) Emission spectra of **1** (0.3 mg) by gradual addition of HA (1 mM) at room temperature (inset: photographs of **1** before and after the addition of HA under UV light (254 nm)). (b) Luminescence response time of **1** after the addition of HA. (c) Luminescence intensities of **1** toward HA in the existence of other various urine components. (d) Emission intensities of **1** toward HA after five cycles.

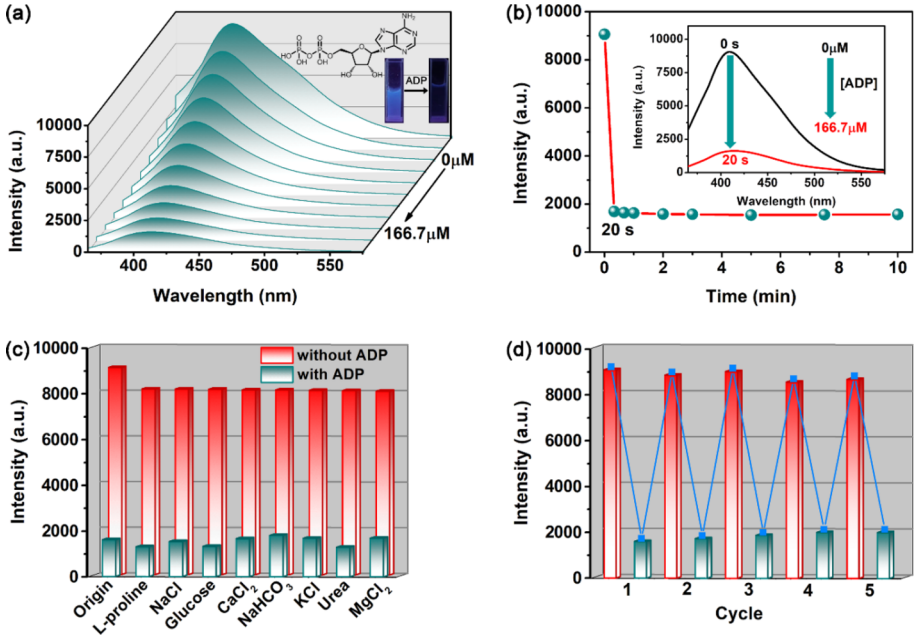

Figure 4. (a) Emission spectra of **1** (0.3 mg) by gradual addition of ADP (1 mM) at room temperature (inset: photographs of **1** before and after the addition of ADP under UV light (254 nm)). (b) Luminescence response time of **1** after the addition of ADP. (c) Luminescence intensities of **1** toward ADP in the existence of other various serum components. (d) Emission intensities of **1** toward ADP after five cycles.

stability of **1** may be attributed to the 2-fold interpenetrating structure.[42]

3.3. Luminescence Detection of HA. The good stability of complex **1** inspired us to explore its potential for luminescence detection in aqueous media. As shown in Figure 3a, the luminescence intensity of **1** dispersed in water decreases with the increase in HA concentration. When the concentration of HA reaches 166.7 μM, the quenching efficiency on **1** is 82.1%. The control experiments with ligands treated with HA show that HA exhibits a small variation in the luminescence intensity of ligands, indicating the good potential of **1** for HA sensing (Figures S7a and S8a). The quenching efficiency can also be studied by the Stern−Volmer (S−V) equation: $I_0/I = K_{SV}[A] + 1$, in which I_0 and I represent the luminescence intensities in the absence and presence of an analyte, respectively, K_{SV} is the quenching constant (M^{-1}), and [A] refers the molar concentration of the analyte. The S−V plot for HA shows a nearly linear correlation at low concentrations (Figure S9), giving a K_{SV} value of 9.9×10^3 M^{-1}. Then, the plot gradually deviates from linearity and bends

https://doi.org/10.1021/acs.inorgchem.2c01313
Inorg. Chem. 2022, 61, 11243−11251

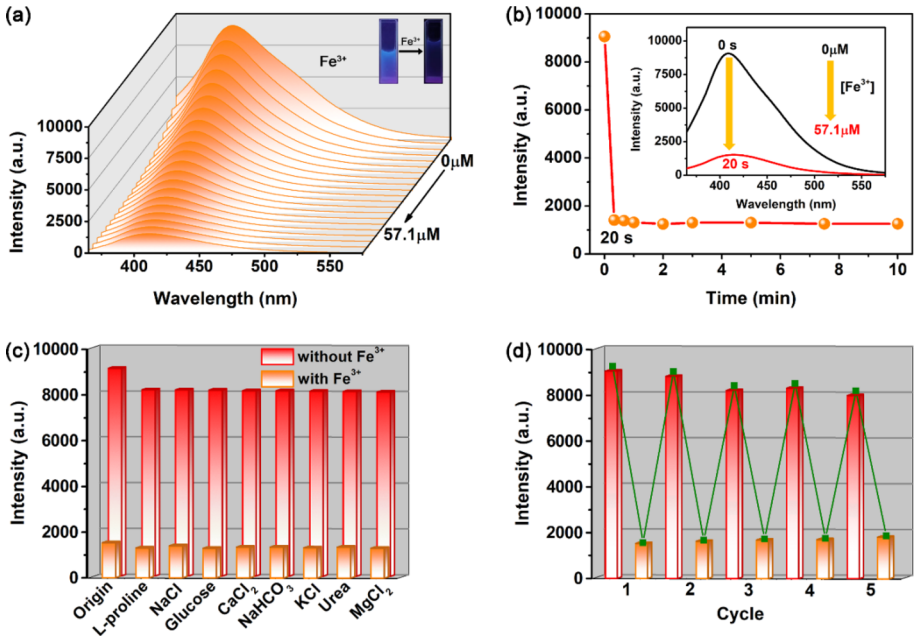

Figure 5. (a) Emission spectra of **1** (0.3 mg) by gradual addition of Fe^{3+} (0.2 mM) at room temperature (inset: photographs of **1** before and after the addition of Fe^{3+} under UV light (254 nm)). (b) Luminescence response time of **1** after the addition of Fe^{3+}. (c) Luminescence intensities of **1** toward Fe^{3+} in the existence of other various serum components. (d) Emission intensities of **1** toward Fe^{3+} after five cycles.

upward at higher concentrations. The limit of detection (LOD = $3\sigma/k$, σ = standard deviation for five repeated blank determinations and k = slope of the calibration curve) for HA is determined to be 1.02 μM (0.18 μg mL^{-1}), which is better than those of previously reported MOFs (Table S4).[3,4,27,32] More importantly, the LOD is lower than the biological exposure index of HA in urine (2.0 mg mL^{-1}) recommended by the American Conference of Governmental Industrial Hygienists (ACGIH),[3] indicating that the complex **1** can be effectively used as a sensitive biosensor for detection of HA in the diagnosis of toluene exposure-related diseases.

The response time is extremely important for the practical application of the biosensors. Therefore, the luminescence response rate of **1** toward HA was investigated by the time-dependent sensing experiment. The emission intensity of HA is significantly reduced within 20 s and remained stable as the time increased (Figure 3b), which is much faster than that of a reported MOF for HA detection (Table S4).[4] The fast response time demonstrates that the complex **1** has great application potential in real-time detection of HA in clinical diagnosis. Considering that urine contains more than one kind of substance, the anti-interference performance of **1** for HA was further explored. The competition experiments were performed by measuring its luminescent intensity to HA in the presence of other urine components such as creatinine, creatine, urea, uric acid, SO_4^{2-}, Na^+, K^+, NH_4^+, Cl^-, and glucose. As shown in Figure 3c, no significant changes in the emission intensity of **1** induced by HA is observed in the existence of other urine components, confirming the anti-interference ability of **1** for detecting HA. Good recyclability is a significant performance marker for the biosensor to assess the practicability. Thus, the recycling experiment of **1** was also carried out. The quenching efficiency of recycled **1** toward HA is significantly unchanged even after five detection cycles (Figure 3d). Meanwhile, the PXRD pattern of the multiple recycled **1** demonstrates that the structure remained unchanged after five cycles (Figure S10). These results indicate its good recyclability and stability for the actual detection application.

3.4. Luminescence Detection of Nucleoside Phosphates. The rapid, sensitive, selective, and recyclable sensing ability of HA prompted us to use the complex **1** to detect nucleotide phosphates such as adenosine monophosphate (AMP), adenosine diphosphate (ADP), and adenosine triphosphate (ATP). As shown in Figure 4a and Figures S11a and S12a, ADP, AMP, and ATP exhibit high quenching effects on **1** with quenching efficiencies of 82.3, 74.9, and 56.9%, respectively. In the control experiments, two ligand solutions titrated by ADP, AMP, and ATP only show a small change in luminescence intensity, suggesting the good sensing ability of **1** toward ADP, AMP, and ATP (Figures S7b–d and S8b–d). Similar to HA detection, the S–V plots of ADP, AMP, and ATP show a good linear relationship at low concentrations and a nonlinear feature at higher concentrations (Figures S13–S15). The K_{SV} values for ADP, AMP, and ATP from the linear fitting of the plots are 1.1×10^4, 1.0×10^4, and 6.4×10^3 M^{-1}, respectively. These data indicate that ADP exhibits high luminescence quenching of the emission for **1** in comparison with the other two biocongeners. The detection limit of **1** toward ADP is further studied, and the LOD for ADP is determined to be 0.95 μM (0.43 μg mL^{-1}), which is better than those of previously reported sensors (Table S5).[43−45]

To demonstrate the response rate of **1** as a biosensor for detection of nucleotide phosphates, the time-dependent sensing experiments of **1** toward nucleotide phosphates were implemented. As shown in Figure 4b and Figures S11b and S12b, the luminescence intensities of **1** are immediately quenched after adding nucleotide phosphates for 20 s, and the intensities remain unchanged as time goes on. The response time is faster than those of other reported studies (Table S5),[8,46] revealing the fast response ability of **1** toward nucleotide phosphates. Similarly, since serum also contains many substances, it is necessary to evaluate the anti-

https://doi.org/10.1021/acs.inorgchem.2c01313
Inorg. Chem. 2022, 61, 11243−11251

interference ability of **1** for the detection of nucleotide phosphates. Competition experiments show that the addition of other serum components such as L-proline, urea, Na^+, K^+, Mg^{2+}, Ca^{2+}, Cl^-, HCO_3^-, and glucose does not influence the luminescence quenching ability of **1** caused by nucleotide phosphates (Figure 4c and Figures S11c and S12c), confirming the high anti-interference ability of **1** for detection of nucleotide phosphates even in the coexistence of other serum components. The recyclability of the detection performance of **1** toward nucleotide phosphates was studied by the cyclic experiments. As shown in Figure 4d and Figures S11d and S12d, the luminescence intensity and quenching efficiency of recycled **1** almost return to the initial level during five sensing cycles. Moreover, the PXRD pattern of the recycled **1** indicates that the structure is not damaged after five recycles (Figure S10). These experiments reveal that **1** can exhibit a recyclable detection ability toward nucleotide phosphates.

3.5. Luminescence Detection of Fe^{3+}. Additionally, the detection capacity of **1** toward the Fe^{3+} ion was also studied. The luminescence titration experiment was performed upon incremental addition of Fe^{3+} ion. As shown in Figure 5a, the emission intensity of **1** is gradually quenched by increasing the concentration of Fe^{3+}. While the Fe^{3+} concentration is 57.1 μM, the quenching efficiency reaches to 86.1%. Control experiments using ligands show relatively weak luminescence responses, proving the good detection performance of **1** on Fe^{3+} (Figures S7e and S8e). Furthermore, the S−V plot shows a good linear relationship at the low concentration and then departs from the linear relation at the high concentration (Figure S16). The K_{SV} value for the Fe^{3+} ion is 3.5×10^4 M^{-1} based on the linear S−V plot. The LOD of **1** for the Fe^{3+} ion is 0.29 μM (0.43 μg mL^{-1}), which falls below those of the reported MOFs for Fe^{3+} detection (Table S6).[47−53] What is more, the LOD is much lower than the normal concentration of Fe^{3+} ion in human serum (5−39 μM),[54] which shows that **1** is a useful biosensor for practical detection of the Fe^{3+} level in the human fluids.

The response rate of **1** to Fe^{3+} was also measured at different time intervals. The luminescence intensity is quenched instantly within the initial 20 s (Figure 5b), which is faster than those of other MOF-based biosensors for Fe^{3+} (Table S6).[50,51,55−57] The fast response sensing ability promotes the application of **1** in real-time detection of Fe^{3+} in clinical diagnosis. Furthermore, we also studied the anti-interference ability of **1** for detection of Fe^{3+}. The presence of other serum components has a negligible effect on the quenching effect of Fe^{3+} ion (Figure 5c), which exhibits that **1** has a high anti-interference ability for Fe^{3+} detection. In addition, the recyclable ability of **1** was also investigated. The repeatable luminescence sensing performance and unchanged PXRD of recycled **1** demonstrate that **1** has good recyclability without the loss of the crystalline structure after five sensing cycles (Figure 5d and Figure S10).

3.6. Application to Real Water Samples. In order to better realize the clinical application, the detection ability of **1** in urine and serum was explored. The luminescence titration experiment of **1** dispersed in urine was performed by the addition of HA. The luminescence intensity gradually declines with increasing concentration of HA (Figure S17a), and this result is similar to the detection of HA in water. The luminescence spectra of **1** dispersed in serum were also recorded by the addition of ADP, AMP, ATP, and Fe^{3+}. As shown in Figures S18a−S21a, the quenching trends are almost consistent with the detection performance in aqueous solution. In addition, the relationship curves of the I_0/I and the concentrations of the abovementioned analytes can be followed in the S−V equation (Figures S17b−S21b), which are more like linear correlations in water. The LOD values of HA, ADP, and Fe^{3+} are determined to be 1.07, 1.16, and 0.40 μM, respectively, which are lower than those of the previously reported studies.[3,4,27,32,43−45,47−53] These results indicate that the complex **1** has great practical potential in biological or clinical target detection.

To further evaluate the reliability and feasibility of **1** for detection in biological media, the urine or serum samples with different concentrations of HA, ADP, AMP, ATP, and Fe^{3+} were measured, and the results are shown in Table S7. The satisfactory recoveries (94.69−107.82%) and relative standard deviations (0.29−4.72%) are obtained in real urine or serum samples, which demonstrates the potential applicability of **1** as a biosensor for the accurate detection of HA, ADP, AMP, ATP, and Fe^{3+} in real biological samples.

3.7. Sensing Mechanism Analysis. To understand the excellent luminescence quenching effect of **1** toward HA, ADP, AMP, ATP, and the Fe^{3+} ion, the possible mechanisms were investigated systematically. First, PXRD patterns of **1** before and after five detection cycles were performed, and the unchanged PXRD patterns confirm that the structure of **1** still retains its integrity (Figure S10), excluding the possibility of quenching caused by structural collapse. To better figure out the sensing mechanism, the UV−vis spectra of HA, ADP, AMP, ATP, and the Fe^{3+} ion were measured. Almost no overlap between the emission spectrum of **1** and the absorption spectra of HA, ADP, AMP, ATP, and the Fe^{3+} ion was observed (Figure S22), revealing the absence of a resonance energy transfer mechanism. However, the excitation spectrum of **1** shows an overlap with the absorption spectra of HA, ADP, AMP, ATP, and the Fe^{3+} ion (Figure S23), indicating that the quenching effect of **1** caused by HA, ADP, AMP, ATP, and the Fe^{3+} ion may be ascribed to the internal filtration effect (IFE) mechanism. Especially, the absorption spectra of nucleotide phosphates exhibit that ADP has the highest absorbance, resulting in the strongest quenching effect of **1** for ADP among these nucleotide phosphates, which is consistent with the experimental results. The observed luminescence quenching effect of **1** toward HA, ADP, AMP, and ATP may be explained by the photoinduced electron transfer (PET) effect. The lowest unoccupied molecular orbital (LUMO) energy level of the MOF is higher than that of the analyte, which facilitates electron transfer from the MOF to the analyte, leading to the quenching of luminescence. The highest occupied molecular orbitals (HOMOs) and LUMOs of HA, ADP, AMP, and ATP were calculated by density functional theory at the B3LYP/6-31G* level. According to previous studies,[58−60] the HOMO and LUMO energies of **1** were obtained by cyclic voltammetry (CV) data (Figure S24). As shown in Figure S26, the LUMO levels of HA, ADP, AMP, and ATP are lower than that of **1**, indicating that the electrons can be transferred from **1** to HA, ADP, AMP, and ATP. In addition, to understand whether the luminescence quenching is caused by the static or dynamic mechanism, the luminescence lifetimes of **1** were recorded before and after the addition of HA, ADP, AMP, ATP, and the Fe^{3+} ion. As shown in Figures S27−S29, the unchanged lifetimes demonstrate the existence of static quenching during the sensing processes, further indicating the formation of the

https://doi.org/10.1021/acs.inorgchem.2c01313
Inorg. Chem. 2022, 61, 11243−11251

nonemissive ground-state complexes between **1** and HA, ADP, AMP, ATP, and Fe^{3+}. For HA, ADP, AMP, and ATP, the carboxylic group of HA and the phosphate group of nucleotide phosphates may be bound to N−H fragments of the urea group through two N−H···O hydrogen bonding interactions.[36] Meanwhile, for the Fe^{3+} ion, the uncoordinated N-donor and O-donor atoms of the urea group in the L^{2-} ligand may bind with Fe^{3+}, which is similar to that reported in another previous study.[37] Moreover, these interactions may facilitate the electron transfer from the MOF to the abovementioned analytes, resulting in a strong quenching effect.

4. CONCLUSIONS

In summary, a stable luminescent 2-fold interpenetrating 3D Cd-MOF (**1**) has been successfully synthesized from a urea-functionalized H_2L ligand, pillared bpbix ligands, and the Cd^{2+} ion *via* a solvothermal method. The complex **1** has good stability in aqueous solutions with pH from 4 to 8 and physiological fluids. Interestingly, the complex **1** dispersed in water simultaneously exhibits selective and recyclable detection of HA, nucleoside phosphates, and the Fe^{3+} ion with a low LOD and fast response time. Importantly, the complex **1** can be used for the accurate and reliable monitoring of HA, nucleoside phosphates, and the Fe^{3+} ion in real urine and serum. This study provides a promising path to achieve multiresponsive luminescent MOF-based biosensors for practical applications in clinical diagnosis and analysis of diseases.

■ ASSOCIATED CONTENT

Supporting Information

The Supporting Information is available free of charge at https://pubs.acs.org/doi/10.1021/acs.inorgchem.2c01313.

Crystal data, structures, TG, PXRD, and other luminescence data (PDF)

Accession Codes

CCDC 2161267 contains the supplementary crystallographic data for this paper. These data can be obtained free of charge via www.ccdc.cam.ac.uk/data_request/cif, or by emailing data_request@ccdc.cam.ac.uk, or by contacting The Cambridge Crystallographic Data Centre, 12 Union Road, Cambridge CB2 1EZ, UK; fax: +44 1223 336033.

■ AUTHOR INFORMATION

Corresponding Author

Hegen Zheng − *State Key Laboratory of Coordination Chemistry, School of Chemistry and Chemical Engineering, Collaborative Innovation Center of Advanced Microstructures, Nanjing University, Nanjing 210023, P. R. China*; orcid.org/0000-0001-8763-9170; Email: zhenghg@nju.edu.cn

Authors

Mingyuan Lei − *State Key Laboratory of Coordination Chemistry, School of Chemistry and Chemical Engineering, Collaborative Innovation Center of Advanced Microstructures, Nanjing University, Nanjing 210023, P. R. China*

Fayuan Ge − *State Key Laboratory of Coordination Chemistry, School of Chemistry and Chemical Engineering, Collaborative Innovation Center of Advanced Microstructures, Nanjing University, Nanjing 210023, P. R. China*

Complete contact information is available at: https://pubs.acs.org/10.1021/acs.inorgchem.2c01313

Notes

The authors declare no competing financial interest.

■ ACKNOWLEDGMENTS

This work was supported by the National Natural Science Foundation of China (no. 21771101).

■ REFERENCES

(1) Park, H. M.; Lee, S. H.; Chung, H.; Kwon, O. H.; Yoo, K. Y.; Kim, H. H.; Heo, S. C.; Park, J. S.; Tae, G. S. Immunochromatographic analysis of hippuric acid in urine. *J. Anal. Toxicol.* **2007**, *31*, 347−353.

(2) Hu, C.; Yang, Z.; Yan, F. H.; Sun, B. C. Extraction of the toluene exposure biomarkers hippuric acid and methylhippuric acid using a magnetic molecularly imprinted polymer, and their quantitation by LC-MS/MS. *Microchim. Acta* **2019**, *186*, 135.

(3) Zhao, J. J.; Zhang, L.; Liu, P. Y.; Chen, W. Z.; Liu, Z. L.; Wang, Y. Q. Water-stable Cd(II)/Zn(II) coordination polymers as recyclable luminescent sensors for detecting hippuric acid in simulated urine for indexing toluene exposure with high selectivity, sensitivity and fast response. *Dalton Trans.* **2021**, *50*, 553−561.

(4) Hao, J. N.; Yan, B. Recyclable lanthanide-functionalized MOF hybrids to determine hippuric acid in urine as a biological index of toluene exposure. *Chem. Commun.* **2015**, *51*, 14509−14512.

(5) Hargrove, A. E.; Nieto, S.; Zhang, T. Z.; Sessler, J. L.; Anslyn, E. V. Artificial Receptors for the Recognition of Phosphorylated Molecules. *Chem. Rev.* **2011**, *111*, 6603−6782.

(6) Qin, L.; Wang, X. Y.; Liu, Y. F.; Wei, H. 2D-Metal-Organic-Framework-Nanozyme Sensor Arrays for Probing Phosphates and Their Enzymatic Hydrolysis. *Anal. Chem.* **2018**, *90*, 9983−9989.

(7) Gao, X.; Liu, J.; Zhuang, X.; Tian, C.; Luan, F.; Liu, H.; Xiong, Y. Incorporating copper nanoclusters into a zeolitic imidazole framework-90 for use as a highly sensitive adenosine triphosphate sensing system to evaluate the freshness of aquatic products. *Sens. Actuators, B* **2020**, *308*, No. 127720.

(8) Zhou, X.; Li, J.; Tan, L.-L.; Li, Q.; Shang, L. Novel perylene probe-encapsulated metal-organic framework nanocomposites for ratiometric fluorescence detection of ATP. *J. Mater. Chem. B* **2020**, *8*, 3661−3666.

(9) Zhang, Y.; Gao, Y. G.; Shi, Y. D.; Tan, L. Q.; Yue, J. S.; Lu, Z. L. [12]aneN_3-based BODIPY as a selective and sensitive off-on sensor for the sequential recognition of Cu^{2+} ions and ADP. *Chin. Chem. Lett.* **2015**, *26*, 894−898.

(10) Goswami, R.; Mandal, S. C.; Seal, N.; Pathak, B.; Neogi, S. Antibiotic-triggered reversible luminescence switching in amine-grafted mixed-linker MOF: exceptional turn-on and ultrafast nanomolar detection of sulfadiazine and adenosine monophosphate with molecular keypad lock functionality. *J. Mater. Chem. A* **2019**, *7*, 19471−19484.

(11) Mu, X.; Qi, L.; Dong, P.; Qiao, J.; Hou, J.; Nie, Z.; Ma, H. Facile one-pot synthesis of L-proline-stabilized fluorescent gold nanoclusters and its application as sensing probes for serum iron. *Biosens. Bioelectron.* **2013**, *49*, 249−255.

(12) Wu, K. Y.; Qin, L.; Fan, C.; Cai, S. L.; Zhang, T. T.; Chen, W. H.; Tang, X. Y.; Chen, J. X. Sequential and recyclable sensing of Fe^{3+} and ascorbic acid in water with a terbium(III)-based metal-organic framework. *Dalton Trans.* **2019**, *48*, 8911−8919.

(13) Cui, Y.; Yue, D.; Huang, Y.; Zhang, J.; Wang, Z.; Yang, D.; Qian, G. Photo-induced electron transfer in a metal-organic framework: a new approach towards a highly sensitive luminescent probe for Fe^{3+}. *Chem. Commun.* **2019**, *55*, 11231−11234.

(14) Dwivedi, A.; Srivastava, M.; Srivastava, A.; Srivastava, S. K. Synthesis of high luminescent Eu^{3+} doped nanoparticle and its application as highly sensitive and selective detection of Fe^{3+} in real water and human blood serum. *Spectrochim. Acta A* **2021**, *260*, No. 119942.
(15) Moein, M. M.; El-Beqqali, A.; Javanbakht, M.; Karimi, M.; Akbari-adergani, B.; Abdel-Rehim, M. On-line detection of hippuric acid by microextraction with a molecularly-imprinted polysulfone membrane sorbent and liquid chromatography-tandem mass spectrometry. *J. Chromatogr. A* **2014**, *1372*, 55−62.
(16) Kongtip, P.; Vararussami, J.; Pruktharathikul, V. Modified method for determination of hippuric acid and methylhippuric acid in urine by gas chromatography. *J. Chromatogr., B* **2001**, *751*, 199−203.
(17) Zuppi, C.; Rossetti, D. V.; Vitali, A.; Vincenzoni, F.; Giardina, B.; Castagnola, M.; Messana, I. Determination of urinary hippuric acid by micellar electrokinetic capillary chromatography. *J. Chromatogr., B* **2003**, *793*, 223−228.
(18) Charter, N. W.; Kauffman, L.; Singh, R.; Eglen, R. M. A generic, homogenous method for measuring kinase and inhibitor activity via adenosine 5′-diphosphate accumulation. *SLAS Discovery* **2006**, *11*, 390−399.
(19) Datta, D.; Meshik, X.; Mukherjee, S.; Sarkar, K.; Choi, M. S.; Mazouchi, M.; Farid, S.; Wang, Y. Y.; Burke, P. J.; Dutta, M.; Stroscio, M. A. Submillimolar Detection of Adenosine Monophosphate Using Graphene-Based Electrochemical Aptasensor. *IEEE Trans. Nanotechnol.* **2017**, *16*, 196−202.
(20) Wu, C.; Wang, S.; Luo, X.; Yuan, R.; Yang, X. Adenosine triphosphate responsive metal-organic frameworks equipped with a DNA structure lock for construction of a ratiometric SERS biosensor. *Chem. Commun.* **2020**, *56*, 1413−1416.
(21) Andersen, J. E. T. A novel method for the filterless preconcentration of iron. *Analyst* **2005**, *130*, 385−390.
(22) Pozebon, D.; Scheffler, G. L.; Dressler, V. L.; Nunes, M. A. G. Review of the applications of laser ablation inductively coupled plasma mass spectrometry (LA-ICP-MS) to the analysis of biological samples. *J. Anal. At. Spectrom.* **2014**, *29*, 2204−2228.
(23) Lustig, W. P.; Mukherjee, S.; Rudd, N. D.; Desai, A. V.; Li, J.; Ghosh, S. K. Metal-organic frameworks: functional luminescent and photonic materials for sensing applications. *Chem. Soc. Rev.* **2017**, *46*, 3242−3285.
(24) Allendorf, M. D.; Bauer, C. A.; Bhakta, R. K.; Houk, R. J. T. Luminescent metal-organic frameworks. *Chem. Soc. Rev.* **2009**, *38*, 1330−1352.
(25) Dong, J.; Zhao, D.; Lu, Y.; Sun, W. Y. Photoluminescent metal-organic frameworks and their application for sensing biomolecules. *J. Mater. Chem. A* **2019**, *7*, 22744−22767.
(26) Zhang, Q.; Wang, C. F.; Lv, Y. K. Luminescent switch sensors for the detection of biomolecules based on metal-organic frameworks. *Analyst* **2018**, *143*, 4221−4229.
(27) Du, Y.; Li, X.; Zheng, H.; Lv, X.; Jia, Q. Design of a calix[4]arene-functionalized metal-organic framework probe for highly sensitive and selective monitor of hippuric acid for indexing toluene exposure. *Anal. Chim. Acta* **2018**, *1001*, 134−142.
(28) Li, X.; Zhou, S.; Lu, S.; Tu, D.; Zheng, W.; Liu, Y.; Li, R.; Chen, X. Lanthanide Metal-Organic Framework Nanoprobes for the In Vitro Detection of Cardiac Disease Markers. *ACS Appl. Mater. Interfaces* **2019**, *11*, 43989−43995.
(29) Hai, X. M.; Li, N.; Wang, K.; Zhang, Z. Q.; Zhang, J.; Dang, F. Q. A fluorescence aptasensor based on two-dimensional sheet metal-organic frameworks for monitoring adenosine triphosphate. *Anal. Chim. Acta* **2018**, *998*, 60−66.
(30) Zhang, D. C.; Li, X. A Zn(II) complex with large channels based on 3′-nitro-biphenyl-3,5,4′-tricarboxylic acid: synthesis, crystal structure, fluorescence sensing of ATP, ADP, GTP, and UTP in aqueous solution and drug delivery. *CrystEngComm* **2017**, *19*, 6673−6680.
(31) Zhao, X. J.; Fang, J. M.; Li, Y. F.; Huang, C. Z. Highly selective recognition of adenosine 5′-triphosphate against other nucleosides triphosphate with a luminescent metal-organic framework of $[Zn(BDC)(H_2O)_2]_n$ (BDC = 1,4-benzenedicarboxylate). *Sci. China: Chem.* **2013**, *56*, 1651−1657.
(32) Qin, S. J.; Hao, J. N.; Xu, X. Y.; Lian, X.; Yan, B. Highly sensing probe for biological metabolite of benzene series pollutants based on recyclable Eu^{3+} functionalized metal-organic frameworks hybrids. *Sens. Actuators, B* **2017**, *253*, 852−859.
(33) Han, L. J.; Kong, Y. J.; Zhang, X. M.; Hou, G. Z.; Chen, H. C.; Zheng, H. G. Fluorescence recognition of adenosine triphosphate and uric acid by two Eu-based metal-organic frameworks. *J. Mater. Chem. C* **2021**, *9*, 6051−6061.
(34) Huang, F.; Hao, G.; Wu, F.; Feng, G. Fluorescence sensing of ADP over ATP and PPi in 100% aqueous solution. *Analyst* **2015**, *140*, 5873−5876.
(35) Rath, B. B.; Vittal, J. J. Water Stable Zn(II) Metal-Organic Framework as a Selective and Sensitive Luminescent Probe for Fe(III) and Chromate Ions. *Inorg. Chem.* **2020**, *59*, 8818−8826.
(36) Amendola, V.; Fabbrizzi, L.; Mosca, L. Anion recognition by hydrogen bonding: urea-based receptors. *Chem. Soc. Rev.* **2010**, *39*, 3889−3915.
(37) Wu, X.; Niu, Q.; Li, T. A novel urea-based "turn-on" fluorescent sensor for detection of Fe^{3+}/F^- ions with high selectivity and sensitivity. *Sens. Actuators, B* **2016**, *222*, 714−720.
(38) Jiang, Y.; Dong, J.; Li, R.; Sun, F.; Wu, H. Channel regulation through solvents for Cd-MOFs based on *p*-methoxyphenyl imidazole dicarboxylate: Synthesis, crystal structure, fluorescence, and explosive identification. *J. Chin. Chem. Soc.* **2022**, 301−309.
(39) Shi, Y. S.; Liu, D.; Fu, L.; Li, Y. H.; Dong, G. Y. Five water-stable luminescent Cd^{II}-based metal-organic frameworks as sensors for highly sensitive and selective detection of acetylacetone, Fe^{3+} and $Cr_2O_7^{2-}$ ions. *CrystEngComm* **2020**, *22*, 4079−4093.
(40) Spek, A. L. Structure validation in chemical crystallography. *Acta Crystallogr. D* **2009**, *65*, 148−155.
(41) Bucens, I. K.; King, R. O. Isospora belli infection and chronic electrolyte disturbance in a child with fetal alcohol syndrome. *Med. J. Australia* **2000**, *173*, 252−255.
(42) Zhang, Q.; Lei, M.; Kong, F.; Yang, Y. A water-stable homochiral luminescent MOF constructed from an achiral acylamide-containing dicarboxylate ligand for enantioselective sensing of penicillamine. *Chem. Commun.* **2018**, *54*, 10901−10904.
(43) Velázquez-Castillo, R. V.; Salomón-Flores, M. K.; Viviano-Posadas, A. O.; Bazany-Rodríguez, I. J.; Bustos-Brito, C.; Bautista-Renedo, J. M.; González-Rivas, N.; Rosales-Vázquez, L. D.; Dorazco-González, A. Recognition and visual detection of ADP and ATP based on a dinuclear Zn(II)-complex with pyrocatechol violet in water. *Dyes Pigm.* **2021**, *196*, No. 109827.
(44) Xia, P.; Su, Z.; Sun, J.; Li, D.; Huang, X. A Couple of Tripodal and Dipodal Fluorescent Sensors for Sequential "On-Off-On" Response to Cu^{2+} and ATP/ADP Recognition in Aqueous Solution. *ChemistrySelect* **2017**, *2*, 11620−11625.
(45) Kumar, A.; Pandey, R.; Kumar, A.; Gupta, R. K.; Dubey, M.; Mohammed, A.; Mobin, S. M.; Pandey, D. S. Self-assembled copper(II) metallacycles derived from asymmetric Schiff base ligands: efficient hosts for ADP/ATP in phosphate buffer. *Dalton Trans.* **2015**, *44*, 17152−17165.
(46) Shi, F.; Li, Y.; Lin, Z.; Ma, D.; Su, X. A novel fluorescent probe for adenosine 5′-triphosphate detection based on Zn^{2+}-modulated L-cysteine capped CdTe quantum dots. *Sens. Actuators, B* **2015**, *220*, 433−440.
(47) Zhao, Y.; Zhai, X.; Shao, L.; Li, L.; Liu, Y.; Zhang, X.; Liu, J.; Meng, F.; Fu, Y. An ultra-high quantum yield Tb-MOF with phenolic hydroxyl as the recognition group for a highly selective and sensitive detection of Fe^{3+}. *J. Mater. Chem. C* **2021**, *9*, 15840−15847.
(48) Yang, D.; Lu, L.; Feng, S.; Zhu, M. First Ln-MOF as a trifunctional luminescent probe for the efficient sensing of aspartic acid, Fe^{3+} and DMSO. *Dalton Trans.* **2020**, *49*, 7514−7524.
(49) Sun, J.; Guo, P.; Liu, M.; Li, H. A novel cucurbit[6]uril-based supramolecular coordination assembly as a multi-responsive luminescent sensor for Fe^{3+}, $Cr_2O_7^{2-}$ and isoquinoline antibiotics in aqueous medium. *J. Mater. Chem. C* **2019**, *7*, 8992−8999.

https://doi.org/10.1021/acs.inorgchem.2c01313
Inorg. Chem. 2022, 61, 11243−11251

(50) Chen, C. H.; Wang, X. S.; Li, L.; Huang, Y. B.; Cao, R. Highly selective sensing of Fe^{3+} by an anionic metal-organic framework containing uncoordinated nitrogen and carboxylate oxygen sites. *Dalton Trans.* **2018**, *47*, 3452−3458.
(51) Wang, B.; Yang, Q.; Guo, C.; Sun, Y.; Xie, L. H.; Li, J. R. Stable Zr(IV)-Based Metal-Organic Frameworks with Predesigned Functionalized Ligands for Highly Selective Detection of Fe(III) Ions in Water. *ACS Appl. Mater. Interfaces* **2017**, *9*, 10286−10295.
(52) Lv, R.; Li, H.; Su, J.; Fu, X.; Yang, B.; Gu, W.; Liu, X. Zinc Metal-Organic Framework for Selective Detection and Differentiation of Fe(III) and Cr(VI) Ions in Aqueous Solution. *Inorg. Chem.* **2017**, *56*, 12348−12356.
(53) Xu, H.; Gao, J.; Qian, X.; Wang, J.; He, H.; Cui, Y.; Yang, Y.; Wang, Z.; Qian, G. Metal-organic framework nanosheets for fast-response and highly sensitive luminescent sensing of Fe^{3+}. *J. Mater. Chem. A* **2016**, *4*, 10900−10905.
(54) Long, L.; Zhou, L.; Wang, L.; Meng, S.; Gong, A.; Zhang, C. A ratiometric fluorescent probe for iron(III) and its application for detection of iron(III) in human blood serum. *Anal. Chim. Acta* **2014**, *812*, 145−151.
(55) Khezerloo, E.; Mousavi-khoshdel, S. M.; Safarifard, V. Sensitive and selective detection of metal ions and small molecules in aqueous media using a hydrolytically stable amide-functionalized metal-organic framework. *Polyhedron* **2019**, *166*, 166−174.
(56) Zheng, M.; Tan, H.; Xie, Z.; Zhang, L.; Jing, X.; Sun, Z. Fast Response and High Sensitivity Europium Metal Organic Framework Fluorescent Probe with Chelating Terpyridine Sites for Fe^{3+}. *ACS Appl. Mater. Interfaces* **2013**, *5*, 1078−1083.
(57) Hou, G. G.; Liu, Y.; Liu, Q. K.; Ma, J. P.; Dong, Y. B. NbO lattice MOFs based on octahedral M(II) and ditopic pyridyl substituted diketonate ligands: structure, encapsulation and guest-driven luminescent property. *Chem. Commun.* **2011**, *47*, 10731−10733.
(58) Wang, B.; Liu, J. H.; Yu, J. M.; Lv, J.; Dong, C.; Li, J. R. Broad spectrum detection of veterinary drugs with a highly stable metal-organic framework. *J. Hazard. Mater.* **2020**, *382*, No. 121018.
(59) Jung, S. O.; Zhao, Q.; Park, J. W.; Kim, S. O.; Kim, Y. H.; Oh, H. Y.; Kim, J.; Kwon, S. K.; Kang, Y. A green emitting iridium(III) complex with narrow emission band and its application to phosphorescence organic light-emitting diodes (OLEDs). *Org. Electron.* **2009**, *10*, 1066−1073.
(60) Huang, J.; Sun, N.; Dong, Y.; Tang, R.; Lu, P.; Cai, P.; Li, Q.; Ma, D.; Qin, J.; Li, Z. Similar or Totally Different: The Control of Conjugation Degree through Minor Structural Modifications, and Deep-Blue Aggregation-Induced Emission Luminogens for Non-Doped OLEDs. *Adv. Funct. Mater.* **2013**, *23*, 2329−2337.

https://doi.org/10.1021/acs.inorgchem.2c01313
Inorg. Chem. 2022, 61, 11243−11251